Dynamic behaviour of Al-Mg aluminum alloy at a wide range of strain rates

Tsuyoshi Kami[1,*], *Hiroyuki* Yamada[2], and *Nagahisa* Ogasawara[2]

[1]Graduate student, Graduate School of Science and Engineering, National Defence Academy, 1-10-20 Hashirimizu Yokosuka Kanagawa, Japan
[2] School of Systems Engineering, National Defence Academy, 1-10-20 Hashirimizu Yokosuka Kanagawa, Japan

Abstract. The effect of strain rate on mechanical properties of Al-2.3wt.%Mg alloy (AA5021) and commercial pure aluminum (purity 99.7wt.%: A1070) was investigated at room temperature. The tensile tests were conducted at strain rates from 1.0×10^{-4} to 1.0×10^{3} s^{-1}. The universal testing machine was used for strain rate 1.0×10^{-4} to 1.0×10^{-1} s^{-1}. For the strain rate 1.0×10^{0} s^{-1}, the servo-hydraulic testing machine, which was developed by our laboratory, was used. The impact strain rate 1.0×10^{3} s^{-1} was obtained using the split Hopkinson pressure bar method. The pure aluminum showed positive strain rate dependence of material strength at the investigated strain rates. In contrast, the Al-2.3wt.%Mg alloy showed the negative strain rate dependence at strain rates from 1.0×10^{-4} to 1.0×10^{0} s^{-1}. However, Al-2.3wt.%Mg alloy showed the positive strain rate dependence at strain rates from 1.0×10^{0} to 1.0×10^{3} s^{-1}. It was surmised that the effect of dislocation locking by the solute Mg atoms became negligible at strain rate of approximately 1.0×10^{0} s^{-1}. It was confirmed that material properties for the Al-Mg alloy at the strain rate of 1.0×10^{0} s^{-1} were important, since the strain rate dependence changed negative to positive around this strain rate.

1 Introduction

Many constitutive equations has been proposed considering the strain rate and temperature effect [1]. In those equations, the flow stress is expressed as a function of various parameters as follows:

$$\sigma = f(\varepsilon, n, Y, \dot{\varepsilon}, T)$$

where ε is the strain, n is the work hardening rate, Y is the yield stress, $\dot{\varepsilon}$ is the strain rate and T is the temperature.

Typically, experiments were conducted using an universal testing machine for the quasi-static strain rate and the split Hopkinson pressure bar method (SHPB)[2,3] for the high strain rate. However, material properties at the dynamic strain rate ($\dot{\varepsilon}=10^{0}\sim10^{1}$ s^{-1}) were barely investigated. It is known that the flow stress starts to increase rapidly at the dynamic strain rate. Thus, the material properties at those strain rates are important.

Until now, the AA5xxx series aluminium alloy has been tested at various strain rates and temperatures. This alloy contains the solute Mg atoms and has the high strength and the corrosion resistance. When the Al-Mg alloy was tested, the serrated flow stress was frequently observed in a stress-strain curve, since the solute Mg atoms interact with the dislocations [4]. This phenomenon is known as the Portevin-Le Chatelier (PLC) effect and dependent on the strain rate and temperature [5].

Previous study showed that the negative strain rate dependence of material strength was observed for Al-Mg alloy at the quasi-static strain rate [4, 6, 7]. In contrast, the positive strain rate dependence has been confirmed for the high strain rate [7, 8]. These are due to the effect of the solute Mg atoms, which can effectively lock the dislocation at the low strain rate and moderate temperature (e.g. room temperature). However, as increasing the strain rate, interaction between the Mg atom and the dislocations decrease [7, 8]. The strain rate at which the strain rate dependence turns negative to positive is not clear. For AA5182 (contained 4.5wt.%Mg), the strain rate dependence was negative at the strain rate lower than 1.0×10^{-1} s^{-1} [4]. Another study for the same alloy showed that the strain rate dependence was negative up to the strain rate of 1.0×10^{0} s^{-1} and turned positive at 7.5×10^{2} s^{-1} [7]. Thus, it is necessary to conduct an experiment at dynamic strain rates for the Al-Mg alloy.

In the present study, the dynamic behaviour of commercial pure aluminum (A1070) and Al-2.3wt.%Mg alloy (AA5021) was investigated at the wide ranges of strain rates in order to clarify the effect of the strain rate on the material properties. In particular, effect of solute Mg atom was discussed.

* Corresponding author: kamimechnda@gmail.com

2 Experiment

2.1 Specimen

The chemical compositions of investigated alloys were listed in Table 1. The AA5021 contained 2.28 wt.% Mg atoms. For comparison, the pure aluminum A1070 was also tested. The specimen geometry was shown in Fig.1. The gauge length of specimen was 8mm and its diameter was ϕ5mm. The specimens were annealed at 618 K in air. The annealing time was 3.6 ks for A1070 and 7.2 ks for AA5021, respectively. After those times, the specimens were furnace cooled to the room temperature.

2.2 Quasi-static tensile test

The quasi-static tensile tests were performed at room temperature using the universal testing machine (Instron, 5500R). The initial strain rates were chosen from 1.0 $\times 10^{-4}$ to 1.0×10^{-1} s^{-1}.

2.3 Dynamic tensile test

The dynamic tensile test was conducted at room temperature using the servo-hydraulic testing machine, which was developed by our laboratory. The configuration of the testing apparatus is shown in Fig.2. The displacement of specimen was measured using the laser displacement sensor (KEYENCE, LK-H155). The sampling rate was 100 kHz. Typical output of this machine is shown in Fig.3(a). Firstly, the piston moved downward without the load in order to stabilize the flow of hydraulic system (indicated as "A" in Fig.3.). Then, since the piston pulled the moving rod, the tensile load was applied to the specimen ("B"). Additionally, the displacement increased with plastic deformation ("C"). The specimen deformation was calculated by subtracting outputs of two displacement sensor (sensors ①, ②). Because the pressure of the servo-hydraulic system slightly increased during a test, the strain rate was also increased as shown in Fig.3(b). The average strain rate during the test was calculated.

2.4 Impact tensile test

The split Hopkinson pressure bar (SHPB) method [2,3] was used for impact tensile test. Figure 4 shows that the configuration of the SHPB apparatus. Main components of this apparatus are a striker, an incident bar, a transmitted bar. After the striker impacts the yoke, the tensile stress wave propagates through the incident bar. When the wave reaches the specimen, part of it is reflected at the specimen and remaining part propagates through the transmitted bar. Those waves were measured using a foil strain gauge (KYOWA, KFG-2-120-C1-16) and semiconductor strain gauge (KYOWA, KSP-1-350-E4), which attached to the incident and transmitted bar, respectively. The sampling rate was 1MHz.

By applying the one-dimensional elastic wave propagation theory, we can derive the nominal stress ($\sigma(t)$), the nominal strain($\varepsilon(t)$), and the strain rate ($\dot{\varepsilon}(t)$) in the specimen as follows:

Table 1. Chemical compositions of investigated alloy (wt.%).

Alloy	Si	Fe	Cu	Mn	Mg	Cr	Zn	Ti	Al
1070	0.04	0.18	0.00	0.00	0.00	0.00	0.00	0.01	99.77
5021	0.13	0.27	0.07	0.25	2.28	0.03	0.03	0.03	Bal.

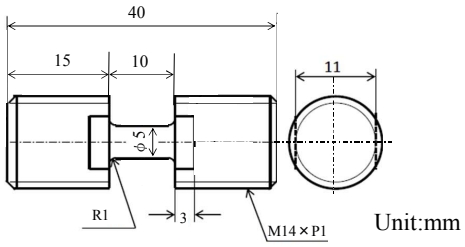

Fig. 1. Geometry of the specimen.

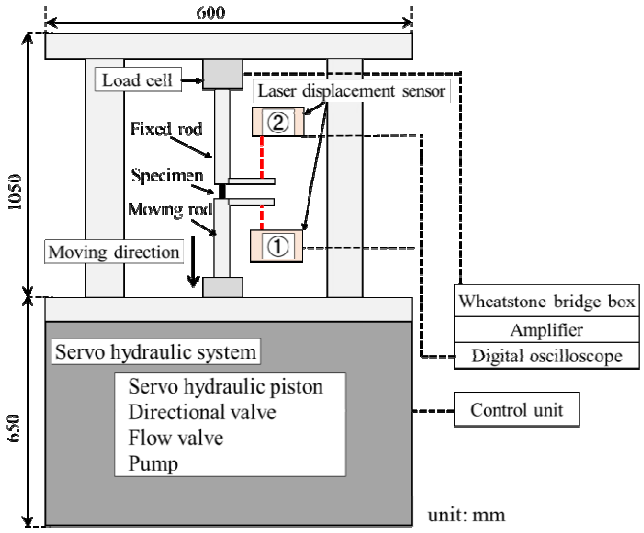

Fig. 2. Configuration of the servo-hydraulic testing apparatus.

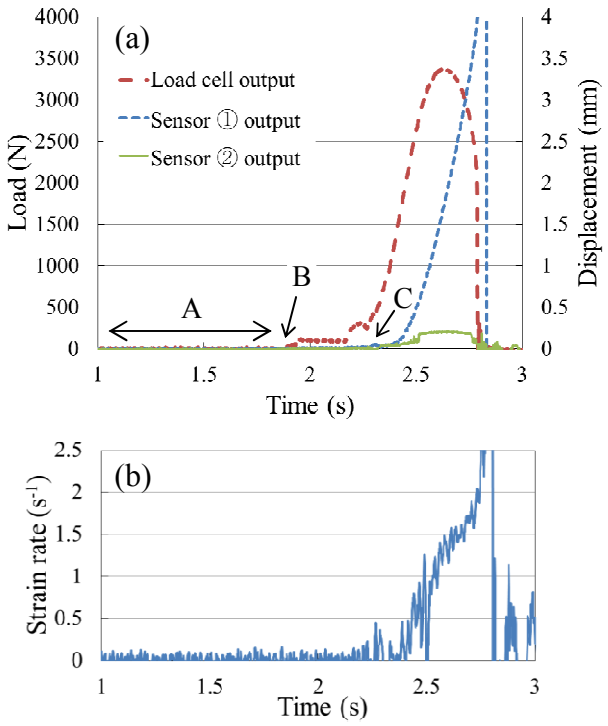

Fig. 3. Typical output of the servo-hydraulic testing appratus. (a) load and two displacement sensor output, (b) calculated strain rate.

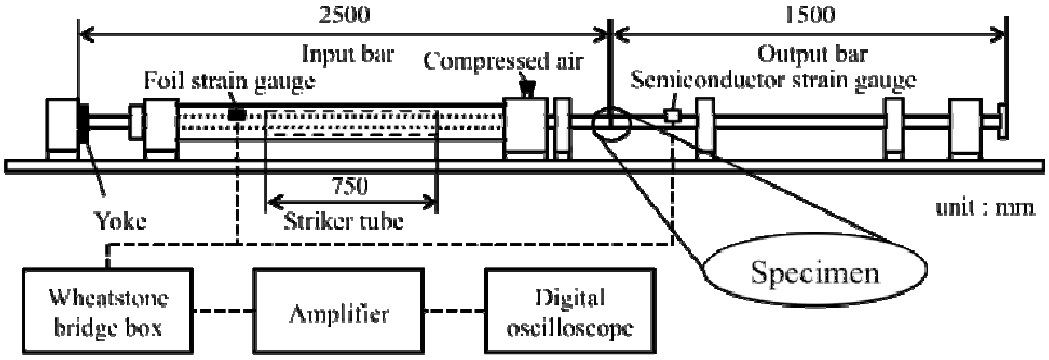

Fig. 4. Configuration of the SHPB.

$$\sigma(t) = \frac{AE}{A_s}\varepsilon_t(t) \quad (1)$$

$$\varepsilon(t) = \frac{2c_0}{l_s}\int_0^t [\varepsilon_i(t) - \varepsilon_t(t)]\,dt \quad (2)$$

$$\dot{\varepsilon}(t) = \frac{2c_0}{l_s}[\varepsilon_i(t) - \varepsilon_t(t)] \quad (3)$$

where A_s is the cross-sectional area of specimen, A is the cross sectional area of the bars, E is Young's modulus of the incident and transmitted bars. c_0 is the velocity of the elastic wave. l_s is the gauge length of the specimen. $\varepsilon_i(t)$ and $\varepsilon_t(t)$ are the incident and transmitted waves, respectively. The average strain rate during the test was calculated from the equation (3).

3 Results

The stress-strain relationship of the A1070 is shown in Fig.5. In addition, the flow stress and strain rate relationship at true strain 0.05, 0.1 and 0.2 is shown in Fig.6. The flow stress increased significantly as increasing the strain rate. It can be said that the A1070 showed the positive strain rate dependence of the material strength, which is common behaviour of the pure aluminum [9]. Figure 7 shows stress-strain relationship of the AA5021. The flow stress and strain rate relationship of this alloy at true strain 0.05, 0.1, 0.15 and 0.2 can be seen in Fig.8.

In contrast to the A1070, the flow stress of the AA5021 decreased from the strain rate 1.0×10^{-4} to 1.0×10^{0} s^{-1} and increased at the impact strain rate ($\dot{\varepsilon}$=7.9×10^{2} s^{-1}). It was surmised that the negative strain rate dependence of the material strength was observed at strain rates from 1.0×10^{-4} to 1.0×10^{0} s^{-1}. However, the strain rate dependence was positive at strain rates from 1.0×10^{0} to 7.9×10^{2} s^{-1}. The strain rate effect for both materials was different, since the AA5021 contained the solute Mg atoms, which was known to interact with dislocations. The effect of the solute Mg atoms will be discussed in the following section.

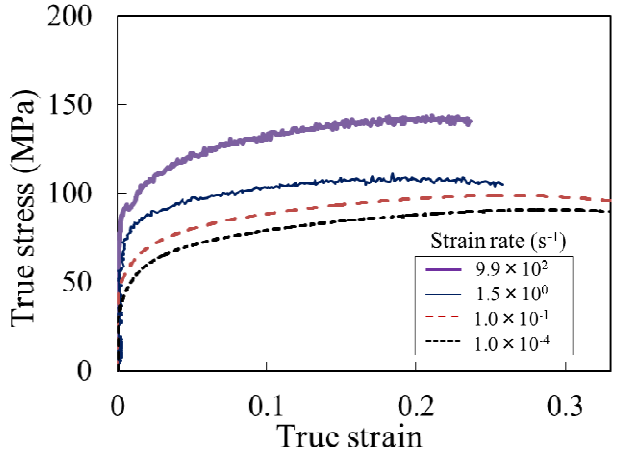

Fig. 5. Stress and strain relationship of 1070 aluminum.

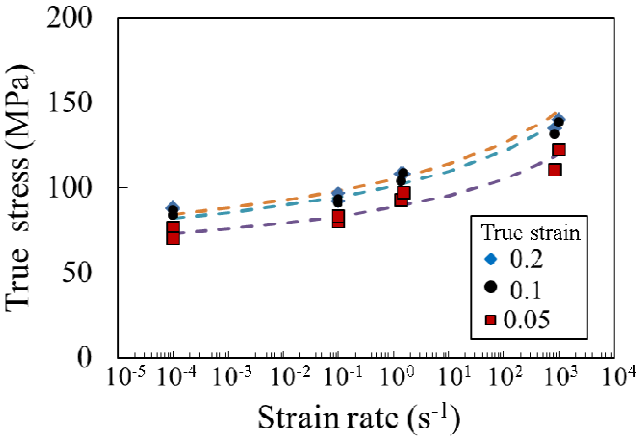

Fig. 6. Stress and strain rate relationship of 1070 aluminum.

4 Discussion

4.1 Previous studies for theory of serration

In the previous study, the following mechanism for the occurrence of the serration has been proposed [10, 11]. Firstly, the movement of the dislocations is prevented by obstacles (e.g. forest dislocation and solute atom). Secondly, the dislocations are temporarily arrested for a certain amount of time (waiting time, t_w). Finally, the dislocations overcome the obstacles and move to another

obstacles. These processes will be repeated and the movement of dislocation may be discontinuous due to the interaction with the solute Mg atoms.

During the waiting time t_w, the solute Mg atoms can move to the dislocations and temporarily lock them. The waiting time is related to the strain rate as follows [10, 11].

$$t_w = \frac{\rho b L}{\dot{\varepsilon}} \quad (4)$$

where ρ is the dislocation density, b is the Burgers vector, L is the average distance between obstacles. If the dislocations are sufficiently locked by the solute Mg atoms, the serrations start to appear [10]. The condition for serration to occur can be expressed as follows [10,12].

$$t_w \geq t_a \quad (5)$$

where t_a is the require time for the solute Mg atoms to fully lock the dislocations. It is said that if the t_w is less than t_a, the smooth flow stress can be seen [10]. Additionally, previous study suggested that the negative strain rate dependence was closely related with the occurrence of the serration [4].

4.2 Strain rate effect on AA5021 results

In the present study, the clear serrations were only observed for the AA5021 at strain rate from 1.0×10^{-4} to 1.0×10^{-2} s^{-1}. From equation (4), it can be said that t_w is sufficiently larger than t_a at the low strain rate. This resulted in the negative strain rate dependence at the low strain rate because of the Mg atoms-dislocation interaction. In such cases, the large force was necessary to break the atmosphere of Mg atoms. As the strain rate increased ($t_w < t_a$), the solute Mg atom and dislocation interaction decrease [10]. In fact, the smooth stress-strain curve was observed at strain rate 1.0×10^{-1} s^{-1}.

It is known that the deformation of metals at the high strain rate can be understood by the thermal activation theory of dislocation motion [13]. In this theory, overcoming the short range obstacles (e.g. forest dislocation) is dependent on the value of the strain rate. The deformation of pure aluminum is governed by this theory [9], which is also inferred from Fig.6. For the AA5021 at high strain rate, the flow stress increased at strain rates from 1.0×10^{0} to 7.9×10^{2} s^{-1}. This suggests that the deformation mechanism of the AA5021 at those strain rates is similar to the one of A1070. At the high strain rate, the thermal activation theory is the dominant mechanism since the Mg atoms cannot migrate to the dislocation at such high strain rate.

As discussed the above, the effect of the solute Mg atoms is dependent on the strain rate. This significantly affects the mechanical properties of the AA5021. In order to determine strain rate dependence of the material strength, it is important to obtain the material properties at the wide range of strain rate. In particular, the dynamic strain rate from 10^{0} to 10^{1} s^{-1} is very important, because the strain rate dependence of this alloy changed at those strain rates and significantly affects development of the constitutive equation.

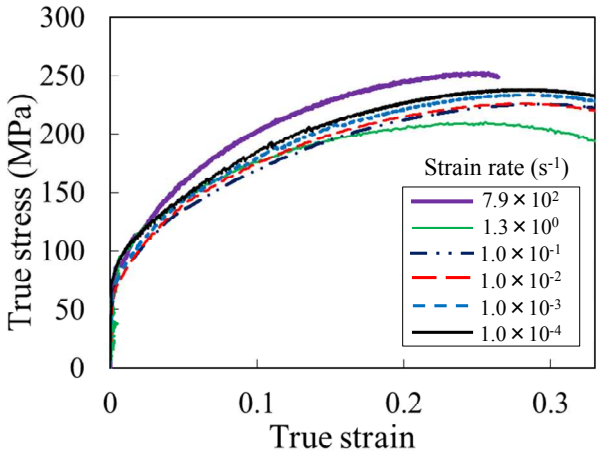

Fig. 7. Stress and strain relationship of 5021 aluminum alloy.

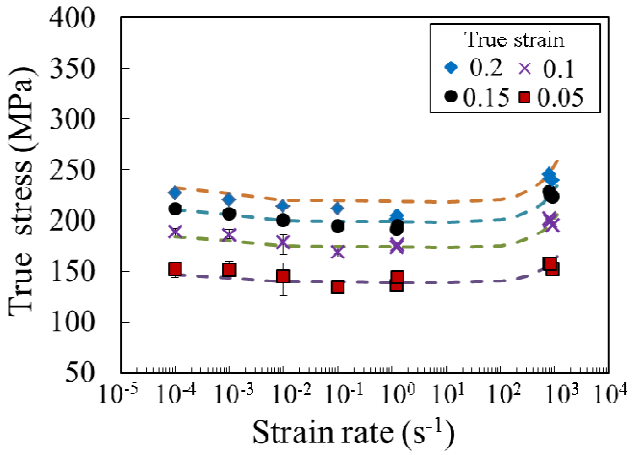

Fig. 8. Stress and strain rate relationship of 5021 aluminum alloy.

5 Conclusion

The strain rate effect on mechanical properties of the A1070 and AA5021 was investigated at room temperature. It was confirmed that the strain rate dependence of AA5021 changed negative to positive at the strain rate from 1.0×10^{0} to 7.9×10^{2} s^{-1}. Thus, it can be said that obtaining dynamic strain rate from 10^{0} to 10^{1} s^{-1} is important for this alloy in order to clarify the strain rate effect of this alloy.

Authors would like to thank UACJ Corporation for providing the AA5021 material.

References

1. H. Huh, K. Ahn, J.H. Lim, H.W. Kim, L.J. Park, *J. Mater. Process. Technol.* **214**, 7, pp.1326–1340 (2014)
2. B. Hopkinson, *Philos. Trans. R. Soc. London A Math. Phys. Eng. Sci.* **213**, 497-508, pp.437–456 (1914)
3. H. Kolsky, *Proc. Phys. Soc. Sect. B*. **62**, 11, pp.676 (1949)

4. R.C. Picu, G. Vincze, F. Ozturk, J.J. Gracio, F. Barlat, A. M. Maniatty, *Mater. Sci. Eng. A*. **390**, 1-2, pp.334–343 (2005)
5. B.J. Brindley, P.J. Worthington, *Acta Metall.* **17**, 11, pp.1357–1361 (1969)
6. A. Rusinek, J.A. Rodríguez-Martínez, *Mater. Des.* **30**, 10, pp.4377–4390 (2009)
7. F. Kabirian, A.S. Khan, A. Pandey, *Int. J. Plast.* **55**, pp.232–246 (2014)
8. E.L. Huskins, B. Cao, K.T. Ramesh, *Mater. Sci. Eng. A*. **527**, 6, pp.1292–1298 (2010)
9. S. Huang, A.S. Khan, *Int. J. Plast.* **8**, 5, pp.501–517 (1992)
10. P.G. McCormigk, *Acta Metall.* **20**, 3, pp.351–354 (1972)
11. L.P. Kubin, Y. Estrin, *Acta Metall. Mater.* **38**, 5, pp.697–708 (1990)
12. C. Wang, Y. Xu, E. Han, *Front. Mater. Sci. China*. **1**, 1, pp.105–108 (2007)
13. F.C. Salvado, F. Teixeira-Dias, S.M. Walley, L.J. Lea, J.B. Cardoso, *Prog. Mater. Sci.* **88**, pp.186–231, (2017)